

Photon and dilepton emission rates from high density quark matter

Prashanth Jaikumar, Ralf Rapp and Ismail Zahed

Department of Physics and Astronomy, SUNY at Stony Brook, New York 11794-3800

(May 21, 2019)

We compute the rates of real and virtual photon (dilepton) emission from dense QCD matter in the color-flavor locked (CFL) phase, focusing on results at moderate densities (3-5 times the nuclear saturation density) and temperatures $T \simeq 80$ MeV. We pursue two approaches to evaluate the electromagnetic (e.m.) response of the CFL ground state: (i) a direct evaluation of the photon self energy using quark particle/-hole degrees of freedom, and (ii) a Hidden Local Symmetry (HLS) framework based on generalized mesonic excitations where the ρ meson is introduced as a gauge boson of a local SU(3) color-flavor group. The ρ coupling to generalized two-pion states induces a finite width and allows to address the issue of vector meson dominance (VMD) in the CFL phase. We compare the calculated emissivities (dilepton rates) to those arising from standard hadronic approaches including in-medium effects. For rather large superconducting gaps (several tens of MeV at moderate densities), as suggested by both perturbative and nonperturbative estimates, the dilepton rates from CFL quark matter turn out to be very similar to those obtained in hadronic many-body calculations, especially for invariant masses above $M \simeq 0.3$ GeV. A similar observation holds for (real) photon production.

I. INTRODUCTION

Recent extensive studies of QCD at finite quark chemical potential (μ_q) have established that the ground state at large densities and zero temperature is a color superconductor with large pairing gaps on the order of 100 MeV (see, e.g. ref. [1] and references therein). Specifically, for 3 flavors of massless quarks, general arguments based on free energy minimization and maximal symmetry favor the formation of a condensate that effectively locks rotations in color and flavor space [2,3]. Among the intriguing implications of this color-flavor locking (CFL) are the modifications of photon propagation in such matter, e.g., true electromagnetism being a combined rotation of the standard $U(1)_Q^{em}$ and $U(1)_Y$ color hypercharge. The color-flavor locked medium is thus transparent to this rotated photon [4]. More recent studies have addressed the question of reflection and refraction at the interface of normal (pairing-free) and CFL media [5]. Given a finite (small) temperature, a natural question would be to ask for the blackbody radiation of the system, i.e., how much a block of CFL matter shines via emission of real photons or dileptons (virtual photons). For photons, the answer is pertinent to photon dynamics in neutron stars with possibly large quark cores that may be condensed into a color superconductor. The fact that rotated photons can propagate freely through the quark core if it is in the superconducting state implies that they can transport energy outward from the core thus providing an efficient cooling mechanism for the core. In turn, the outer layers of the star, most likely characterized by larger opacities, may heat up significantly.

Apart from consequences for specific physical systems like neutron stars, one ought to address the issue of photon and dilepton emission at varying temperature and baryon density as a general means to investigate different regions of the QCD phase diagram, especially in colder and denser regions. The latter may be accessible to the HADES experiment at GSI [6]. Small final state interactions make photon and dilepton probes important long lived signatures of the state of strongly interacting matter. Corresponding production rates have been extensively studied for both hot hadronic matter incorporating medium effects [7–14] (see ref. [15] for a recent review) as well as for the Quark-Gluon Plasma using perturbative [16–20] and nonperturbative [21–23] approaches. It has been pointed out that perturbative $q\bar{q}$ annihilation rates in a QGP at comparable temperatures and densities are suggestive of a ‘quark-hadron duality’, i.e., the dilepton signature for an interacting confined phase with broken chiral symmetry resembles that of a QGP with chiral symmetry restored. This has been found for both the low-mass (ρ -/ ω -) region [24] and the intermediate-mass region [25,26] (between the ϕ and J/Ψ). Could such a dual scenario hold for the dense phase of condensed diquarks at finite temperature as well? In this paper, we will address this question by making perturbative estimates of the photon and dilepton emissivities from dense superconducting matter with 3 flavors of massless quarks (the CFL phase). While such perturbative calculations are strictly valid only at parametrically large chemical potential, it is intriguing to extrapolate down to densities of a few times that of normal nuclear matter ($n_0 = 0.16 \text{ fm}^{-3}$). In this way, our approach attacks the finite density problem from the side of large baryon density and serves to complement studies of emission rates from the low density (hadronic) side, extended to include medium effects. Significantly, our calculation at finite density allows for finite temperature effects that are possibly as large as the gaps in the CFL phase, conjectured to be several tens of MeV at $\mu_q \simeq 300\text{--}500$ MeV.

Another issue we have sought to address in our analysis of the dilepton emission rates is the viability of vector meson dominance (VMD) at high density. Along the lines of ref. [27,28] we have included excitations describing the rho meson (ρ) in the CFL phase via an effective theory based on hidden local symmetry. Based on weak coupling analyses to leading logarithm accuracy, effective Lagrangian approaches to QCD in the CFL phase have proven to be useful with applications to color-flavor anomalies, hidden local symmetry and meson properties [27,29,30]. Here, we use the effective Lagrangian to obtain the coupling of the ρ meson to the rotated photon in the CFL phase and model its width in the dense phase via a Breit-Wigner resonance through its coupling to two generalized pions. In this way, we recover VMD and show that the ρ meson makes an important contribution to the dilepton emission rate, much like in low density hadronic frameworks.

The organization of this paper is as follows. In section II, we compute the photon polarization tensor from the quark loop in the CFL phase (independently confirming the result first obtained in ref. [31]), and present numerical estimates for corresponding dilepton and photon rates at finite temperature and for baryon densities down to $n_B = (3-5) n_0$. In section III, we derive the effective Lagrangian for the CFL phase which incorporates hidden local symmetry and show how the generalized ρ meson arises as a dynamical gauge boson of this symmetry. In particular, we address the fate of vector meson dominance in this model, thereby determining the coupling of the generalized vector mode to the photon. Again, we present the associated contribution to the dilepton production rate. In section IV we confront the combined emissivities from CFL matter with prior estimates from in-medium hadronic as well as perturbative QGP calculations. We summarize and conclude in section V.

II. CFL PHASE AND E.M. CURRENT CORRELATOR I: WEAK COUPLING

A. One-Loop Photon Self Energy

The photon polarization tensor in color-flavor locked quark matter to one-loop order was first derived by Litim and Manuel [31]. For the sake of completeness, and as an independent confirmation of their result, we here provide a calculation using a different quark basis than in ref. [31]. In what follows we adopt the notation of ref. [32]. We assume all quarks to be massless. The self energy receives contributions from the diagonal (dressed quasiparticles) and off diagonal (diquark) components of the Nambu-Gorkov propagator which reads [33]

$$S(K) = \begin{pmatrix} G^+(K) & \Xi^-(K) \\ \Xi^+(K) & G^-(K) \end{pmatrix}, \quad (1)$$

where $(G^\pm)^{-1} \equiv G_0^\pm - \Sigma^\pm$, $\Sigma^\pm \equiv \Phi^\mp G_0^\mp \Phi^\pm$, with $\Phi^+ \sim \langle \psi_C \bar{\psi} \rangle$, $\Phi^- \sim \langle \psi \bar{\psi}_C \rangle$ and $(G_0^\pm)^{-1}(K) = \not{K} \pm \mu_q \gamma_0$. ψ_C denotes the charge conjugate partner of ψ . The off-diagonal components of the matrix in eq.(1) are $\Xi^\pm \equiv -G_0^\mp \Phi^\pm G^\pm$. With the convenient choice of $SU(3)$ generators $T^8 = \lambda_8/2 = (\sqrt{3}/2)Q$, ($Q = \text{diag}\{2/3, -1/3, -1/3\}$) and $T^3 = \text{diag}\{0, 1/2, -1/2\}$, the mixing of the photon with the eighth gluon can be described by the linear combinations [31]

$$\tilde{A}_\mu = A_\mu \cos \theta_{CFL} - G_\mu^8 \sin \theta_{CFL} \quad (2)$$

$$\tilde{G}_\mu^8 = A_\mu \sin \theta_{CFL} + G_\mu^8 \cos \theta_{CFL}, \quad (3)$$

where $\tan \theta_{CFL} = 2e/\sqrt{3}g$, and e, g denote the gauge couplings of A_μ, G_μ respectively. The CFL quarks couple to the in-medium photon \tilde{A}_μ with strength $\tilde{e} = e \cos \theta_{CFL}$ via the vertex

$$(\Gamma^\mu)_{ab}^{ij} = (\tilde{Q})_{ab}^{ij} \gamma^\mu = \frac{1}{\sqrt{3}} \left[(\lambda_8)^{ij} \delta_{ab} - \delta^{ij} (\lambda_8)_{ab} \right] \gamma^\mu \quad (4)$$

since $\tilde{Q} = Q \otimes 1 + 1 \otimes Y$ where Y represents the hypercharge operator. In eq. (4), $\{i, j\}$ and $\{a, b\}$ denote flavor- and color-indices, respectively. The self-energy then takes the form

$$\Pi^{\mu\nu}(K) = \frac{\tilde{e}^2}{2} \text{Tr}_{k,s,c,f,NG} \left[\Gamma^\mu S(k + \frac{K}{2}) \Gamma^\nu S(k - \frac{K}{2}) \right], \quad (5)$$

where the traces are to be carried out over internal 4-momentum (k), spin (s), color (c), flavor (f) and Nambu-Gorkov (NG) indices. The NG trace is easily performed in view of eq. (1), whereas the color-flavor locked structure of the condensate is conveniently unraveled using the projectors [34],

$$C_{ab}^{1ij} \equiv \frac{1}{3} \delta_a^i \delta_b^j, \quad C_{ab}^{2ij} \equiv \frac{1}{2} (\delta_{ab} \delta^{ij} - \delta_a^j \delta_b^i), \quad C_{ab}^{3ij} \equiv \frac{1}{2} (\delta_{ab} \delta^{ij} + \delta_a^j \delta_b^i) - C_{ab}^{1ij}. \quad (6)$$

These projectors may be identified with the singlet (P_1) and octet (P_8) ones [35] according to

$$P_1 = C^1, \quad P_8 = C^2 + C^3. \quad (7)$$

Using the following trace relations,

$$\begin{aligned} \text{Tr}_{c,f} [\tilde{Q} P_1 \tilde{Q} P_1] &= 0 = \text{Tr}_{c,f} [\tilde{Q} P_1 \tilde{Q} P_8] = \text{Tr}_{c,f} [\tilde{Q} (C^2 - C^3) \tilde{Q}^T P_1] \\ \text{Tr}_{c,f} [\tilde{Q} P_8 \tilde{Q} P_8] &= 4 = -\text{Tr}_{c,f} [\tilde{Q} (C^2 - C^3) \tilde{Q}^T (C^2 - C^3)], \end{aligned} \quad (8)$$

the self energy of the CFL photon can be expressed in compact form as

$$\Pi^{\mu\nu}(K) = 2\tilde{e}^2 \left[G_{88}^{\mu\nu}(K) + \Xi_{88}^{\mu\nu}(K) \right], \quad (9)$$

with

$$G_{88}^{\mu\nu}(K) = \sum_{e=\pm} \text{Tr}_{k,s} \left(\gamma^\mu G^e(k + \frac{K}{2}) \gamma^\nu G^e(k - \frac{K}{2}) \right) \quad (10)$$

$$\Xi_{88}^{\mu\nu}(K) = \sum_{e=\pm} \text{Tr}_{k,s} \left(\gamma^\mu \Xi^e(k + \frac{K}{2}) \gamma^\nu \Xi^{-e}(k - \frac{K}{2}) \right). \quad (11)$$

This result for $\Pi^{\mu\nu}$ explicitly agrees with the one quoted in ref. [31], cf. eq.(27) therein. The subscript 88 indicates that only the octet projection contributes. The sum over $e = \pm$ encompasses the contributions of particles (+) and antiparticles (-). As the antgap dependent pieces arise only at order $\mathcal{O}(\mu_q^{-2})$ [28], we neglect pairing effects for antiquarks in our calculation of emission rates. Moreover, the antgap is gauge dependent even for forward scattering of antiquarks [36]. We keep, however, the contribution from free antiquarks. This, in particular, has the advantage of naturally recovering the dilepton rate from the perturbative $q\bar{q}$ annihilation process for vanishing quark gaps, which is our baseline for assessing the effects of pairing. The Dirac spin traces may be performed explicitly using equations (45) and (95) of ref. [32]. The 4-momentum trace over k involves a 3-momentum integration as well as a summation over Matsubara frequencies in the energy component k_0 within the imaginary time formalism to incorporate finite temperature effects. This allows to obtain explicit expressions for the various components of $\Pi^{\mu\nu}(K)$ (see ref. [31] for details), which in the following section will be employed to compute photon and dilepton emission rates.

B. Photon and Dilepton Rates

The medium modification of the photon field¹ in the CFL phase is contained in the components of the polarization tensor, which in turn can be related to e.m. emissivities [16,7]. The thermal emission rate of real photons reads

$$q_0 \frac{dR_\gamma}{d^3q} = -\frac{1}{(2\pi)^3} \text{Im} \Pi^{(\text{ret})\mu}_\mu(q_0 = q) f^B(q_0; T), \quad (12)$$

while that for dileptons (virtual photons) is given by

$$\frac{dR_{ee}}{d^4q} = -\frac{\alpha}{12\pi^4 M^2} \text{Im} \Pi^{(\text{ret})\mu}_\mu(q_0, q) f^B(q_0; T), \quad (13)$$

where $f^B(q_0; T) = 1/[\exp(q_0/T) - 1]$ is the thermal Bose factor, $\alpha = e^2/4\pi$ with e the usual electromagnetic charge, and $M^2 = q_0^2 - q^2$ the invariant mass of the lepton pair. The factor of α illustrates that the photon becomes

¹We refer here to the (massless) rotated photon in the CFL phase [37] which plays the role of true electromagnetism.

normal after it emerges from the CFL phase, and then emits a lepton pair. For the sake of simplicity, we do not consider the situation when the dileptons are produced inside the CFL matter itself, in which case the dressing of photons by the lepton pair must be included in the self energy. The imaginary part of the retarded photon self energy, $\text{Im}\Pi^{\text{(ret)}}_{\mu} = \text{Im}\Pi^L + 2\text{Im}\Pi^T$, is the weighted sum of its transverse and longitudinal projections (at the photon point, i.e., for vanishing invariant mass $M^2 = q_0^2 - q^2$, Π^L vanishes). It is obtained from $\Pi^{\mu\nu}(K)$ by performing the appropriate analytic continuation to arbitrary complex values of the external frequency $iK^0 \equiv q_0$. The one-loop result for positive $q_0 > 0$ then reads

$$\begin{aligned} \text{Im}\Pi^{\text{(ret)}}_{\mu} &= \frac{\tilde{e}^2}{2\pi^2} \sum_{e_1, e_2 = \pm} \int d^3k \\ &\times \left\{ \frac{\Delta^2}{2} \left(\frac{\hat{\mathbf{k}}_1 \cdot \hat{\mathbf{k}}_2 - 1}{\epsilon_1 \epsilon_2} \right) \left[\delta(q_0 - \epsilon_1 - \epsilon_2) (1 - N_1 - N_2) + [\delta(q_0 - \epsilon_1 + \epsilon_2) - \delta(q_0 + \epsilon_1 - \epsilon_2)] (N_1 - N_2) \right] \right. \\ &\quad \left. - \left[\delta(q_0 - \epsilon_1 - \epsilon_2) (1 - N_1 - N_2) \left(1 - \frac{\xi_1 \xi_2}{\epsilon_1 \epsilon_2} \right) + [\delta(q_0 - \epsilon_1 + \epsilon_2) - \delta(q_0 + \epsilon_1 - \epsilon_2)] (N_1 - N_2) \left(1 + \frac{\xi_1 \xi_2}{\epsilon_1 \epsilon_2} \right) \right] \right\}, \quad (14) \end{aligned}$$

where the quasiparticle energies are denoted by $\epsilon_i = \sqrt{\xi_i^2 + \Delta^2}$, with $\xi_i = e_i k_i - \mu_q$ and $k_1 = |\vec{k}|$, $k_2 = |\vec{q} - \vec{k}|$ the quasiparticle momenta. $N_i = f^F(\epsilon_i; T) = 1/[\exp(\epsilon_i/T) + 1]$ are the usual Fermi distribution functions which become Θ -functions in the $T=0$ -limit. The summation over all combinations of $e_1 = \pm$ and $e_2 = \pm$ generates a total of 4 contributions embraced in curly brackets. However, since we approximate antiparticles as free (ungapped), the Δ^2 term is zero except for the $e_1 = e_2 = +$. The physical interpretation of the various terms is encoded in the delta functions which determine the on-shell kinematics of the process (in eq. (14), we have omitted terms involving delta functions of the form $\delta(q_0 + \epsilon_1 + \epsilon_2)$, as they do not contribute to the production of on-shell photons or lepton pairs). Let us focus on the contribution of the particles to $\text{Im}\Pi$. At zero temperature, Pauli Blocking enforces the distribution functions to vanish identically, i.e., $N_1 = N_2 = 0$. Thus the only contribution to the imaginary part arises from the $\delta(q_0 - \epsilon_1 - \epsilon_2)$ -terms. For vanishing gap (free quark gas), energy-momentum conservation in the particle-hole excitation implies $M^2 = -2k_1 k_2 (1 + \cos \theta)$ ($\theta = \angle(\vec{k}_1, \vec{k}_2)$), i.e., the response is strictly spacelike which corresponds to standard Landau damping (this obviously remains true for $T > 0$). For a finite gap, the response sets in at $q_0 > 2\Delta$, the break-up of a Cooper pair acting as the threshold for excitations, as expected. More importantly, the response extends into the timelike region as well, which again follows from energy-momentum conservation: choosing, e.g., $\cos \theta = -1$ (which is the optimal configuration for a timelike response), one finds $M^2 = 2(\Delta^2 + \epsilon_1 \epsilon_2 - \xi_1 \xi_2)$ to be positive, thus allowing for photon and dilepton emission. These features are confirmed in Fig. 1, where $\text{Im}\Pi(q_0, q, \Delta; T = 0)$ is plotted versus energy at fixed 3-momentum $q = 60$ MeV and for various values of the gap parameter.

At finite temperature, $N_1, N_2 \neq 0$ and the delta functions with energy arguments $q_0 \mp \epsilon_1 \pm \epsilon_2$ also contribute. The

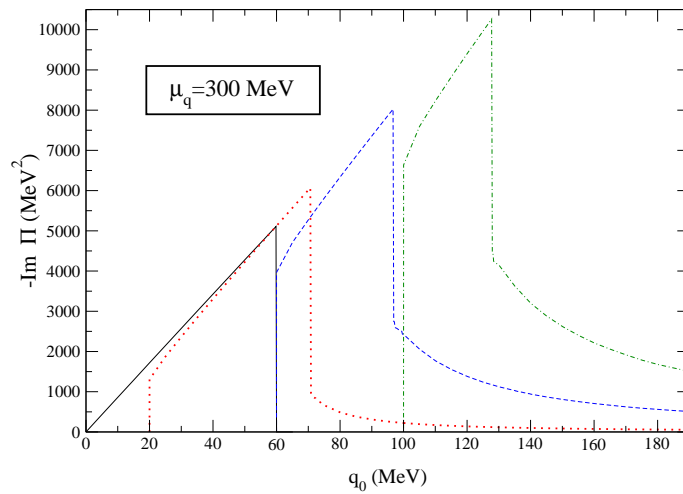


FIG. 1. $\text{Im}\Pi$ at temperature $T = 0$ MeV, three momentum $q = 60$ MeV and for $\Delta = 0$ MeV (solid), $\Delta = 10$ MeV (dotted), $\Delta = 30$ MeV (dashed) and $\Delta = 50$ MeV (dash-dotted). In each case, the response has a threshold at $q_0 = 2\Delta$.

resulting response function as shown in Fig. 2 indicates a significant relocation of strength from the spacelike to the timelike region. Such a feature was also found in ref. [38], where neutrino scattering in the color superconductor has

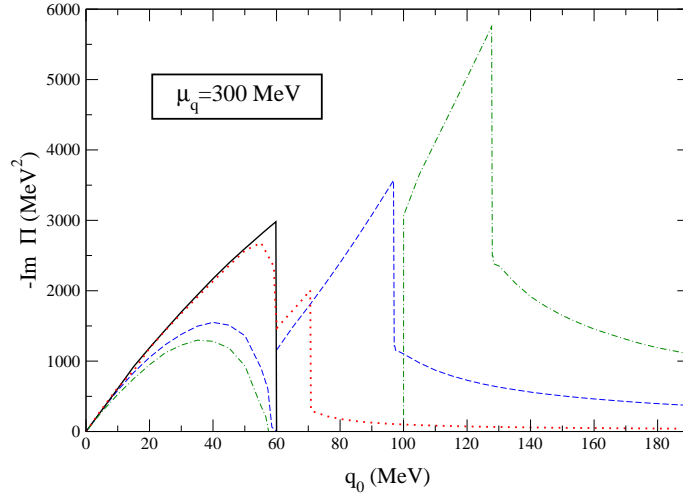


FIG. 2. $\text{Im}\Pi$ at finite temperature $T = 50$ MeV, three momentum $q = 60$ MeV and for $\Delta = 0$ MeV (solid), $\Delta = 10$ MeV (dotted), $\Delta = 30$ MeV (dashed) and $\Delta = 50$ MeV (dash-dotted). The relocation of strength from the spacelike to the timelike region is evident. This signals the possibility of dilepton emission.

been studied. The delta functions with opposing signs on the quasiparticle energies are restricted to spacelike M^2 , and are relevant for scattering of CFL photons off quarks (Landau damping in the CFL phase). In our context of photon and dilepton emission, where $M^2 \geq 0$, these terms are of no direct concern. However, we may note that the shifting of response strength from the spacelike to the timelike region implies the suppression of scattering as compared to the free Fermi gas [38].

To display the associated dilepton emission rates, it is common to focus on the three-momentum integrated quantity which produces the invariant-mass spectrum

$$\frac{dR_{ee}}{dM^2} = \int \frac{d^3q}{2q_0} \frac{dR_{ee}}{d^4q} . \quad (15)$$

The pertinent numerical results for the CFL phase based on the one-loop photon self energy, eq. (14), are displayed in Fig. 3, where only the particle contributions are retained to highlight the impact of Cooper pairing on the emission rate. The curves have been evaluated for a quark chemical potential of $\mu_q = 350$ MeV (corresponding to a baryon density $n_B \simeq 5.4n_0$ including massless strange quarks) assuming a temperature dependence of the gap as inferred from BCS theory,

$$\Delta = \Delta_0 \sqrt{1 - \left(\frac{T}{T_c}\right)^2} . \quad (16)$$

The rather large variation in the considered gap values (10-70 MeV) is motivated by the sharp curvature of the above relation near T_c . For definiteness, using $T_c \simeq 0.56\Delta_0$ with $\Delta_0 \simeq 150$ MeV at $\mu_q \simeq 350$ MeV (as suggested by both perturbative [39] and nonperturbative [3] estimates), the gap increases from a few to several tens of MeV over a small range of temperature around $T = 80$ MeV. The CFL rates are compared to free quark-antiquark annihilation at order α_S^0 in a baryon-rich QGP first computed in ref. [17]:

$$\frac{dR_{q\bar{q} \rightarrow ee}}{d^4q} = \frac{\alpha^2}{4\pi^4} \frac{T}{q} f^B(q_0; T) \sum_{q=u,d,s} e_q^2 \ln \frac{(x_- + \exp[-(q_0 + \mu_q)/T])(x_+ + \exp[-\mu_q/T])}{(x_+ + \exp[-(q_0 + \mu_q)/T])(x_- + \exp[-\mu_q/T])} , \quad (17)$$

with $\alpha = e^2/4\pi$ and $x_{\pm} = \exp[-(q_0 \pm q)/2T]$.² As characteristic for soft emission rates generated from in-medium

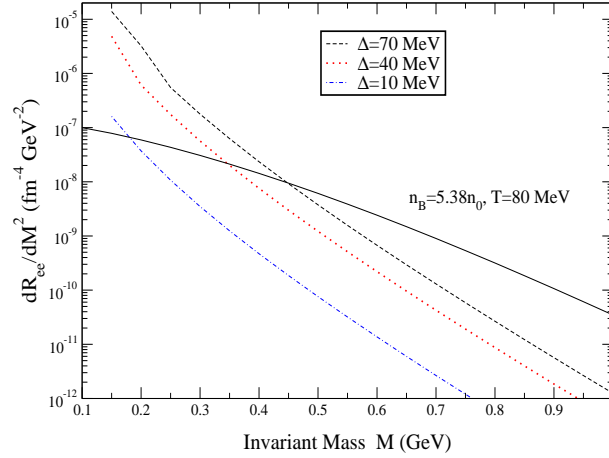


FIG. 3. Dilepton rates at finite gap and finite temperature (with particles only). The rate vanishes as the gap goes to zero. The solid line is the $\mathcal{O}(\alpha_S^0)$ estimate of the free $q\bar{q}$ annihilation rate at the same temperature and density.

effects, the gap-induced processes exhibit a much steeper slope than the perturbative $q\bar{q}$ annihilation, exceeding the latter towards small masses. It is straightforward to incorporate the leading (free) antiparticle contribution within the CFL one-loop results by retaining the antiparticle projectors in the diagonal parts of the Nambu-Gorkov propagator.

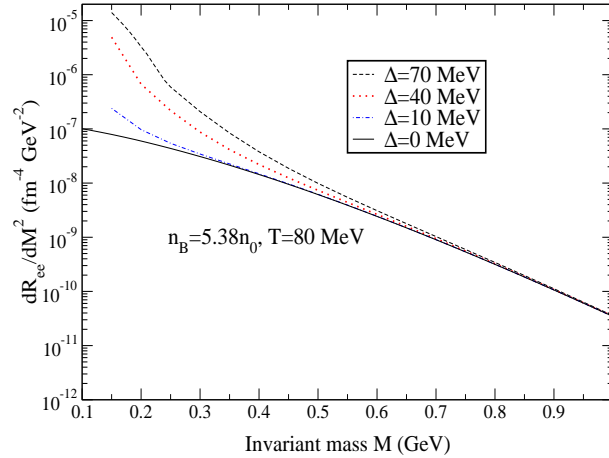


FIG. 4. Dilepton emission rate including the antiparticle contribution. (For $\Delta = 0$ MeV, the perturbative $q\bar{q}$ annihilation rate is recovered.)

Upon doing so we recover the limit of perturbative $q\bar{q}$ annihilation as the gap goes to zero, cf. Fig.4, where also the additional processes due to finite pairing gaps have been included. Whereas the gap acts as a threshold energy ($q_0 \geq 2\Delta$) in the response function, eq.(14), this is not so for the invariant-mass spectrum, as there is no constraint on

²One should note that perturbative corrections arising from soft processes can give substantial enhancement over the lowest-order ($\mathcal{O}(\alpha_S^0)$) result of eq. (17) in the low-mass region ($M < 1$ GeV) region [19]. Qualitatively, such corrections have a similar shape to the ones induced by finite gaps.

the three momentum transfer q . Nevertheless, the energy threshold leaves its traces also in the invariant mass spectra. To illustrate this point, we have magnified in Fig. 5 the region of very low masses $M \leq 0.2$ GeV. An inflection point

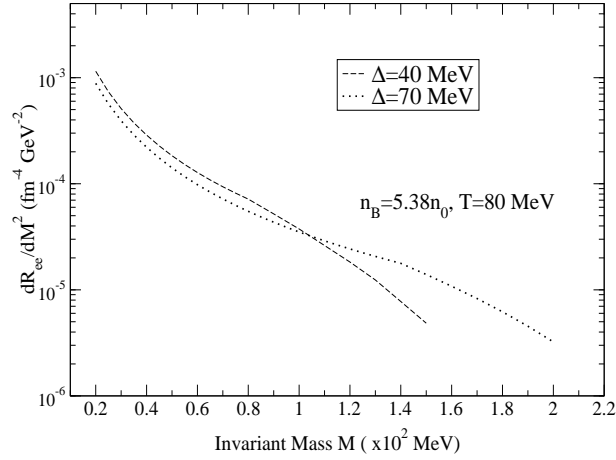


FIG. 5. Dilepton emission rate in the very low mass region. A smooth turning over seems to occur at $M = 2\Delta$.

of the rate is discernible at $M \simeq 2\Delta$, below which a finite 3-momentum transfer is required, entailing a suppression of dilepton production. In fact, the rate with the smaller pairing gap even exceeds the one with the more tightly bound Cooper pairs.

The photon emission rate, eq. (12), from the CFL phase at the same density and temperature ($\mu_q = 350$ MeV, $T = 80$ MeV) is plotted in Fig. 6, where we again compare to the perturbative result in the normal QGP phase. For the

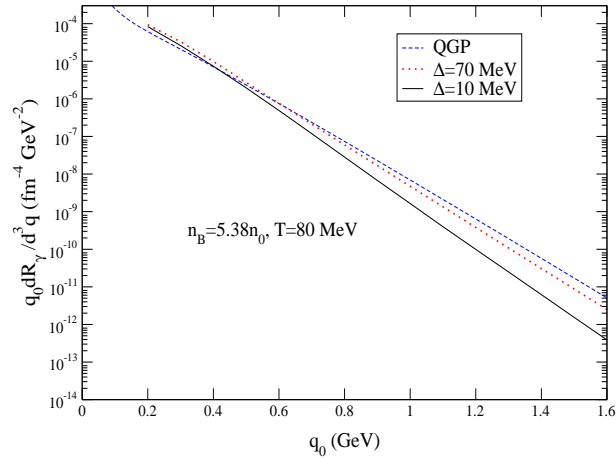


FIG. 6. Direct photon emission rates from gapped quarks in the CFL phase at pairing gaps of 10 and 70 MeV (full and dotted lines, respectively) compared to the complete leading order QGP result from ref. [41] (dashed line).

latter, the complete leading order calculation in the strong coupling constant has recently been given in ref. [41] along with a convenient parameterization which we used to obtain the corresponding curve. Similar to the dilepton case, the corrections from gap formation become (slightly) larger than free QGP emission towards low energies. Beyond energies of 500 MeV, a reasonable agreement persists only for the larger gap value.

III. CFL PHASE AND E.M. CURRENT CORRELATOR II: HIDDEN LOCAL SYMMETRY

A. Generalized Mesons and Effective Lagrangian

Beyond the 1-loop result from the previous section, the existence of mesonic bound states in the vector and axial vector channel in high density QCD [28] is expected to further affect the dilepton emissivity from dense low temperature matter. The knowledge of the coupling of these modes to the electromagnetic current affords us the opportunity to complement studies of dilepton emission from hot and dense hadronic environments with “hadronic-type” rates from the high density side. Starting from a suggestion made in ref. [28], we will here adopt the Hidden Local Symmetry (HLS) approach to construct the coupling of these so-called ‘generalized’ vector mesons in the CFL phase to the photon field. As an effective low energy theory, the HLS framework determines the couplings between generalized vector and pseudoscalar mesons, the latter being the Goldstone modes of chiral symmetry breaking in the CFL phase. This feature also provides the answer to the question whether dilepton production through the generalized vector mesons bears any overlap with the quark one-loop description of the previous section. It turns out that the quark-based (weak coupling) analysis, carried out to leading logarithm accuracy, does not support a coupling to the generalized pseudoscalar states (though it may be finite at next-to-leading order) and moreover, the coupling of the vector excitation to the physical vector current is zero [28]. Therefore, the decay of the generalized vector mesons (or, equivalently, the annihilation of generalized pseudoscalar mesons) adds to the dilepton rate independent of the one-loop result of the previous section. The HLS framework allows us to determine the coupling of the generalized vector mesons to the electromagnetic current, and hence the contribution to the dilepton rate.

The idea of interpreting low-lying vector (and axial vector) mesons in free space as dynamical gauge bosons of a hidden local symmetry originated in refs. [42–45].

A particular advantage of this framework becomes apparent in the conventional $[SU(2)_L \otimes SU(2)_R]_{\text{global}}$ nonlinear sigma model where the electromagnetic interaction can be implemented as a global gauge symmetry, coupling to global isospin charge, distinct from the (hidden) local $SU(2)_V$ charge to which the rho meson (ρ) couples. This separation of the photon source from the ρ allows for a natural explanation of several phenomenological facts (such as ρ dominance of the vector coupling to pions, KSRF relations and universality of the ρ coupling) at the cost of fixing one parameter (the universal vector coupling constant).

In weak coupling, the (composite) generalized vector mesons in the CFL phase are distinct from the screened and Higgsed gluons [28]. Could they be the realization of a hidden local symmetry, besides the explicit local color symmetry? If the Cooper pairs have finite size, there is, strictly speaking, no hidden local invariance in the order parameter apart from explicit color symmetry. However, we will work in the zero size approximation, in which case the condensate does indeed exhibit a hidden local symmetry corresponding to the unbroken color-flavor $SU(3)$ group³. Just like the ρ meson in case of hidden local symmetry at zero density [44], the vector mesons of the CFL phase are composite and heavy. In this respect, our hidden gauge approach is different from ref. [29] wherein the local $SU(3)_c$ was the hidden (color) gauge. In the following we construct an effective Lagrangian for the Nambu-Goldstone bosons arising from the spontaneous symmetry breaking, with the vector mesons introduced as gauge particles of the unbroken local symmetry. As in the vacuum case, they are rendered physical degrees of freedom by postulating a kinetic term (assumed to be generated at the quantum level), which does not affect the low energy dynamics of the theory.

To start the derivation of the HLS Lagrangian in the CFL ground state, we recall that, formally, a nonlinear sigma model based on the coset manifold G/H is gauge equivalent to another model with $G_{\text{global}} \otimes H_{\text{local}}$ symmetry and that the gauge bosons corresponding to the hidden local symmetry in H_{local} are composite fields. For the CFL phase, $G \equiv [SU(3)_C \otimes SU(3)_L \otimes SU(3)_R]_{\text{global}}$ and $H \equiv [SU(3)_{C+L+R}]_{\text{local}}$. In terms of (right-handed) quark fields, the explicit form of the order parameter reads

$$\langle q_{R,\alpha}^{ai} q_{R,\beta}^{bj} \rangle = \frac{1}{2} (C^\dagger \gamma_5 P_R)_{\alpha\beta} (\kappa_1 \delta^{ai} \delta^{bj} + \kappa_2 \delta^{aj} \delta^{bi}) \quad (18)$$

where $\{a, b\}$, $\{i, j\}$ and $\{\alpha, \beta\}$ denote color, flavor and spinor-indices, respectively (C : charge conjugation matrix, P_R : right-handed chiral projector). An equivalent form applies to the left-handed fields. Following refs. [27,28], this symmetry-breaking pattern implies the emergence of 8 Goldstone bosons corresponding to $SU(3)_{c+A}$ -valued

³A similar caveat holds for effective field descriptions of hadrons in the nonperturbative vacuum; it may be overcome by higher order terms in the chiral perturbation series.

condensate rotations of the form $e^{-i\gamma_5\Theta^A T^A}$ with associated group generators T^A ($A = 1, \dots, 8$). In what follows we will assume the CFL ground state to be invariant under the parity transformation. We introduce unitary fields corresponding to the individual left- and right-handed rotations, characterized by expectation values

$$\langle \Phi_{Lai} \rangle = -\langle \Phi_{Rai} \rangle = \delta_{ai} , \quad (19)$$

which implies $\kappa_1 = -\kappa_2$ in eq. (18), and fixes the overall $U(1)$ phases in

$$\Phi_{L,R} \equiv e^{2i\phi_{L,R}} U_{L,R}(x) \quad (20)$$

at, e.g., $\langle \phi_L \rangle = 0$ and $\langle \phi_R \rangle = \pi/2$ ⁴. The generalized left- and right-handed $SU(3)$ fields can be parameterized by

$$U_L(x) = e^{2i\pi_L(x)/F_\pi} \quad (21)$$

$$U_R(x) = e^{2i\pi_R(x)/F_\pi} , \quad (22)$$

where $\pi_{L,R} = \pi_{L,R}^A T^A$, and the $SU(3)$ generators are normalized as $\text{Tr}(T^A T^B) = \delta^{AB}/2$. At this point we have doubled the number of colored (generalized) Goldstone bosons represented by $SU(3)$ phases of U_L and U_R . The latter transform under G as $U_L \rightarrow g_c^* U_L g_L^\dagger$ and $U_R \rightarrow g_c^* U_R g_R^\dagger$, respectively. The following further decomposition,

$$U_L(x) = \xi_c^T(x) \xi_L(x) \quad (23)$$

$$U_R(x) = \xi_c^T(x) \xi_R(x) , \quad (24)$$

then makes explicit the additional invariance under the hidden local symmetry $h \in [SU(3)_{C+L+R}]_{\text{local}}$:

$$\xi_c^T(x) \rightarrow \xi_c^T(x) h^\dagger(x) \quad (25)$$

$$\xi_{L,R}(x) \rightarrow h(x) \xi_{L,R}(x). \quad (26)$$

We will fix the local $SU(3)_{C+L+R}$ gauge by choosing $\xi_c^T(x) = \xi_{L,R}(x) \equiv \xi(x)$. It follows that $\pi_L = \pi_R$, so that we recover the expected number of Goldstone bosons (eight). This simply means that color locks to the flavor diagonal so that left- and right-handed 'pions' are the same. In this way, we implement the description of (generalized) pions as phases of the (colored) diquark condensate, and avoid an explicit appearance of the gluon fields in our effective theory⁵. With this realization, one introduces a vector gauge field V_μ that transforms inhomogeneously under the hidden local symmetry parametrized by $h(x)$. Since the gauge fields may be viewed as connections in the coset manifold, we can define the gauge covariant derivative as

$$D_\mu \xi(x) = \partial_\mu \xi(x) - iV_\mu \xi(x) . \quad (27)$$

The effective Lagrangian for the CFL pions is now assembled from invariants under $SU(3)_C \otimes SU(3)_L \otimes SU(3)_R \otimes [SU(3)_{C+L+R}]_{\text{local}} \otimes (\text{parity})$:

$$\begin{aligned} \mathcal{L}_{eff} = & -\frac{F_T^2}{4} \text{Tr}(D_0 \xi^\dagger \cdot \xi - D_0 \xi \cdot \xi^\dagger)^2 - \frac{F_S^2}{4} \text{Tr}(D_i \xi^\dagger \cdot \xi - D_i \xi \cdot \xi^\dagger)^2 \\ & - a_T \frac{F_T^2}{4} \text{Tr}(D_0 \xi^\dagger \cdot \xi + D_0 \xi \cdot \xi^\dagger - 2iV_0)^2 - a_S \frac{F_S^2}{4} \text{Tr}(D_i \xi^\dagger \cdot \xi + D_i \xi \cdot \xi^\dagger - 2iV_i)^2 + \dots, \end{aligned} \quad (28)$$

where the breaking of Lorentz invariance of the finite density ground state is reflected by individual temporal and spatial pion decay constants F_T and F_S , respectively⁶. The first two terms of eq. (28) reproduce the kinetic term for the pions while the other two (proportional to a_T and a_S) vanish identically utilizing the equation of motion for the V_μ field,

⁴We will not include in our low energy description the breaking of $U(1)_B \rightarrow Z_2$ associated with baryon superfluidity (H -meson) or the anomalous $U_A(1)$ current (η' meson), as they are not relevant to the problem at hand.

⁵In other works, it was the field $\Sigma = U_L^\dagger U_R$ which mapped the meson octet, with gluons acquiring a mass via the gauge fixing of color as the hidden local symmetry. This integrating out of gluons led to an identification with the effective chiral Lagrangian at zero density.

⁶One has $F_T = \sqrt{3}F_S$ using the axial vector current normalization for the pion decay constant [28,30]. Their ratio equals v_π , the velocity of the Goldstone modes. To leading logarithm accuracy, $F_T^2 \simeq \mu^2/\pi^2$ [28,30].

$$V_\mu^a = -i\text{Tr}\{T^a(\partial_\mu\xi \cdot \xi^\dagger + \partial_\mu\xi^\dagger \cdot \xi)\} \quad . \quad (29)$$

As in the zero density case, the vector field propagates by postulating a kinetic term assumed to arise from interactions on the microscopic QCD level. This does not affect the limit of low energy dynamics that the effective Lagrangian is aiming to describe. The ellipsis in eq. (28) denotes higher order and possible mass terms of heavier excitations consistent with the CFL symmetries, which we ignore. With the addition of the gauge kinetic term, and expanding up to $\mathcal{O}(p^2)$ (p : momentum of the pion field), we have

$$\begin{aligned} \mathcal{L}_{eff} = & \frac{1}{2}(\partial_0\boldsymbol{\pi})^2 + \frac{v_\pi^2}{2}(\partial_i\boldsymbol{\pi})^2 + \frac{a_T}{2}\mathbf{V}_0 \cdot \boldsymbol{\pi} \times \partial_0\boldsymbol{\pi} + \frac{a_S}{2}\mathbf{V}_i \cdot \boldsymbol{\pi} \times \partial_i\boldsymbol{\pi} \\ & + \frac{1}{2}(a_T F_T^2)\mathbf{V}_0^2 + \frac{1}{2}(a_S F_S^2)\mathbf{V}_i^2 + \frac{1}{2g_T^2}(\mathbf{F}_{0i})^2 - \frac{1}{2g_S^2}(\mathbf{F}_{ij})^2 + \dots \quad , \end{aligned} \quad (30)$$

where we define the standard field strength tensor $\mathbf{F}_{\mu\nu} = \partial_\mu\mathbf{V}_\nu - \partial_\nu\mathbf{V}_\mu + \mathbf{V}_\mu \times \mathbf{V}_\nu$ ⁷. Upon rescaling the vector fields, $\mathbf{V}_0 \rightarrow g_T\mathbf{V}_0$, $\mathbf{V}_i \rightarrow g_S\mathbf{V}_i$, we identify

$$g_{V_0\pi\pi} = \frac{1}{2} a_T g_T \quad , \quad m_T^2 = a_T g_T^2 F_T^2 \quad , \quad (31)$$

$$g_{V_i\pi\pi} = \frac{1}{2} a_S g_S \quad , \quad m_S^2 = a_S g_S^2 F_S^2 \quad . \quad (32)$$

We note that, apart from Lorentz symmetry breaking, the effective Lagrangian, eq. (30), is formally identical to that obtained at zero density with hidden local symmetry for the chiral $SU(2)_V$ subgroup. For the numerical calculations presented below, the value of g_T will be taken to be that of $g_{\rho\pi\pi}$ in vacuum⁸. We will show later 4-dimensional transversality of the photon self energy requires $g_S = g_T$. Both the mass of the vector field and its coupling to two generalized pions depends on the parameters a_T and a_S . A suggestive choice will emerge when we introduce electromagnetism into our effective theory. This is our next step, so as to assess the coupling of the generalized (neutral) vector mesons to the (modified) photons with application to e.m. spectra.

The true electromagnetic gauge boson in the CFL medium is the modified photon (\tilde{A}_μ), with a modified coupling \tilde{e} to charged degrees of freedom. \tilde{A}_μ is the gauge field associated with local $U(1)_{\tilde{Q}}$ phase transformations on the $U_{L,R}$ fields. Noting that this is equivalent to a simultaneous transformation $\xi_f \rightarrow \xi_f e^{-ieQ\cos\theta}$, $\xi_c \rightarrow \xi_c e^{-igY\sin\theta}$, we see that $U_{L,R}$ transform as

$$U_{L,R} \rightarrow e^{i\tilde{e}Q} U_{L,R} e^{-i\tilde{e}Q} \quad , \quad (33)$$

where we have used $Q = -Y$ for multiplication from the left. Thus, the covariant gauging with electromagnetism can be achieved via

$$D_\mu^{em} \xi_f = \partial_\mu \xi_f + i\tilde{e}\xi_f \tilde{A}Q \quad (34)$$

$$D_\mu^{em} \xi_c^* = \partial_\mu \xi_c^* + i\tilde{e}\xi_c^* \tilde{A}Q \quad (35)$$

(the superscript $*$ denotes complex conjugation). Thus the effective Lagrangian, eq. (30), with electromagnetism incorporated becomes

$$\begin{aligned} \mathcal{L}_{eff}^{em} = & \mathcal{L}_{eff} - \frac{1}{4}(F_{\mu\nu}^{em})^2 - \frac{2\tilde{e}m_T^2}{\sqrt{3}g_T}V_0^8\tilde{A}_0 - \frac{2\tilde{e}m_S^2}{\sqrt{3}g_S}V_i^8\tilde{A}_i + \frac{1}{2}\frac{4\tilde{e}^2m_T^2}{3g_T^2}\tilde{A}_0^2 + \frac{1}{2}\frac{4\tilde{e}^2m_S^2}{3g_S^2}\tilde{A}_i^2 \\ & - (\frac{a_T-2}{\sqrt{3}})\tilde{e}\tilde{A}_0 f_{AB8}\pi^A \partial_0\pi^B - (\frac{a_S-2}{\sqrt{3}})\tilde{e}\tilde{A}_i f_{AB8}\pi^A \partial_i\pi^B + \dots \quad . \end{aligned} \quad (36)$$

It obviously exhibits generalized ρ^0 - $\tilde{\gamma}$ mixing (V^8 is assigned the generalized neutral ρ meson). Vector meson dominance (VMD), i.e., the absence of a direct $\pi\pi\gamma$ vertex, is recovered for $a_T = a_S = 2$, in analogy to free space, where it

⁷Here, boldface notation indicates 8-component vector in flavor-space with the cross- (\times) and dot-products to be read as $(\mathbf{V} \times \mathbf{V})_A = f_{ABC}V^B V^C$ and $\mathbf{V} \cdot \mathbf{V} = V^A V^A$ with f_{ABC} the antisymmetric structure constant of the $SU(3)$ group.

⁸Another estimate of g_T may be obtained by a study of the 4-pion vertex by integrating out the ρ fields in the infinite mass limit.

successfully reproduces the empirical ρ dominance of the electromagnetic pion form factor. Such a parameter choice thus seems natural on account of the formal resemblance of the CFL and vacuum case at the level of the bare effective Lagrangian. On the other hand, it has recently been argued [47], based on a one-loop renormalization group equation (RGE) analysis, that VMD (for $N_f=3$) is only accidentally realized in the chirally broken phase at zero density, and that it does not hold towards the phase boundary of chiral restoration. The CFL phase, however, is a priori of a rather different nature (i.e., its symmetries and physical excitations), so that VMD cannot be precluded by the perturbative arguments invoked in ref. [47].

With VMD enforced, the mass eigenstates of the photon and the vector meson fields follow from eq. (36) via diagonalization,

$$B_\mu = (g^2 + \frac{4}{3}\tilde{e}^2)^{-1/2} \left(g\tilde{A}_\mu + \frac{2}{\sqrt{3}}\tilde{e}V_\mu^8 \right) \quad (37)$$

$$W_\mu^8 = (g^2 + \frac{4}{3}\tilde{e}^2)^{-1/2} \left(gV_\mu^8 - \frac{2}{\sqrt{3}}\tilde{e}\tilde{A}_\mu^8 \right) \quad (38)$$

$$m_B^2 = 0, \quad m_{W^8}^2 = aF^2(g^2 + \frac{4}{3}\tilde{e}^2), \quad (39)$$

where $g = g_T, F = F_T$ for $\mu = 0$ and $g = g_S, F = F_S$ for $\mu = i$. We see that ρ - $\tilde{\gamma}$ mixing spontaneously breaks $[SU(3)]_{\text{hidden}} \otimes U(1)_Q$ down to $U(1)_{em}$.

We have thus shown that the HLS framework, which has proven successful in the chirally broken vacuum state, can be implemented into the (chirally broken, $N_f=3$) high density color superconducting ground state as well. The (generalized) ρ meson emerges as a resonance of generalized two-pion states, with its mass and width determined by the effective Lagrangian eq. (36). We are now in position to evaluate its contribution to the dilepton emission rate in dense CFL matter.

B. Dilepton and Photon Rates

Adopting the VMD hypothesis for the coupling of (real and virtual) CFL photons to the generalized isovector mesonic current (as motivated in the previous section), the electromagnetic correlation function can be saturated by the ρ^0 meson. The pertinent dilepton rate, eq. (13), then takes the form

$$\frac{dR_{ee}}{d^4q} = -\frac{\alpha}{3\pi^3 M^2} \tilde{\alpha} f^\rho(q_0; T) \frac{(m_\rho)^4}{g_{\rho\pi\pi}^2} g_{\mu\nu} \text{Im} D^{\mu\nu}(M, q) \quad (40)$$

with $\tilde{\alpha} = \tilde{e}^2/4\pi$, f^ρ the thermal Bose-Einstein occupation factor, and $g_{\mu\nu} D^{\mu\nu} = D_L + 2D_T$ the in-medium propagator of the generalized ρ meson, summed over its longitudinal and transverse polarizations. The form of this propagator follows from inverting the equations of motion for the spatial and temporal components of the field V_μ ,

$$D^{\mu\nu} = \frac{P_T^{\mu\nu}}{M^2 - m_S^2} + \frac{P_L^{\mu\nu}}{M^2 - m_S^2 \frac{q_0^2}{M^2} + m_T^2 \frac{q^2}{M^2}} + \frac{q^\mu q^\nu}{m_T^2 q_0^2 - m_S^2 q^2}. \quad (41)$$

Here, P_L and P_T are the standard longitudinal and transverse projectors for photons in matter [48]. We note that for $m_T = m_S = m_\rho$, this propagator reduces to that for the massive spin-1 field in the covariant (Landau) gauge,

$$D^{\mu\nu} = \frac{1}{M^2 - m_\rho^2} \left(-g^{\mu\nu} + \frac{q^\mu q^\nu}{m_\rho^2} \right). \quad (42)$$

Though we have made a particular gauge fixing, the gauge parameter would appear only in the $q^\mu q^\nu$ term of eq. (41), and therefore not contribute to the rate by transversality of the photon. The rate is a gauge invariant (observable) quantity, driven by the imaginary parts of the longitudinal and transverse modes, i.e., spectral functions. The transverse propagator has a pole at $M = m_S$, while the longitudinal propagator admits two positive definite solutions. These are given by

$$m_\pm^2 = \frac{m_S^2}{2} \left[1 \pm \sqrt{1 - 4q^2 \frac{m_T^2 - m_S^2}{m_S^4}} \right] \quad (43)$$

As $m_T > m_S$ (cf. footnote 6), there exists a limiting 3-momentum given by $q_{\max} = m_S^2 / (2\sqrt{m_T^2 - m_S^2})$ beyond which the longitudinal mode is damped. The lower mode corresponding to the choice of negative sign in the above equation vanishes at $q = 0$ where it has zero strength, and only the upper mode persists, becoming degenerate with the transverse part, as it must in the rest frame.

We may view the longitudinal mode as having an energy-momentum dependent self-energy by decomposing the inverse propagator as

$$M^2 - m_S^2 \frac{q_0^2}{M^2} + m_T^2 \frac{q^2}{M^2} \equiv M^2 - m_S^2 - \Sigma_L(M, q) \quad (44)$$

$$\Sigma_L(M, q) = -(m_T^2 - m_S^2) \frac{q^2}{M^2}. \quad (45)$$

We impose retarded boundary conditions by continuing the $1/M^2$ factor as $q_0 \rightarrow q_0 - i\epsilon$. To illustrate the above features, we insert a small (finite) imaginary part into the self energy and display real and imaginary part of the longitudinal propagator in Figs. 7 and 8, respectively, for fixed values of the masses ($m_S = 500$ and $m_T = \sqrt{3}m_S$).

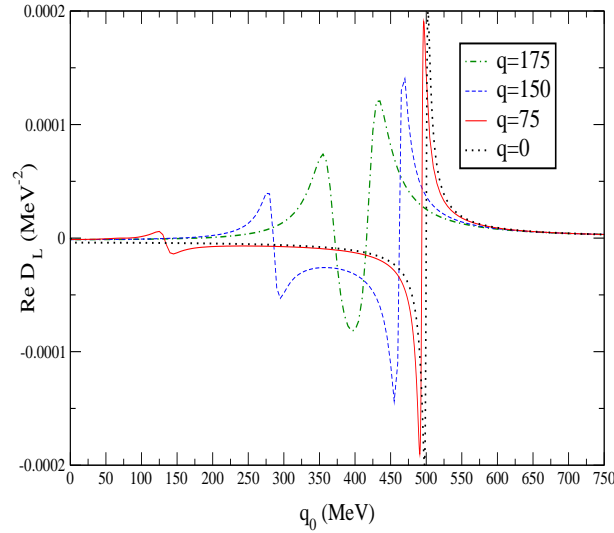


FIG. 7. The real part of the longitudinal ρ propagator as a function of frequency for different 3-momenta q at fixed masses m_S and m_T . The upper and lower modes are degenerate at $q = q_{\max}$ and separate with decreasing q .

For q approaching q_{\max} ($\simeq 176.5$ MeV with our choice of masses), the two modes merge while for smaller q they are distinct. For $q = 0$, only the mode degenerate with the transverse part survives. The retarded boundary condition renders the spectral function,

$$\mathcal{A}_L(\omega) = -2 \text{Im} D_L(\omega) \quad (46)$$

a positive definite quantity (which directly figures into the e.m. rates), even though the lower ('-') mode has a negative discontinuity. We have checked that the spectral sum rule for the two longitudinal modes,

$$\int_{-\infty}^{\infty} \frac{d\omega}{2\pi} \omega \mathcal{A}_L(\omega) = 1 \quad (47)$$

holds for independent values of m_T and m_S .

We can go beyond the mean field results, eq. (41), by including loop corrections from the coupling of the ρ to 2 pions. In that case, the imaginary part of the ρ self-energy diagram (decay width) are ascribed to the $\rho\pi\pi$ interaction, which we evaluate according to the $\rho\pi\pi$ matrix element determined by eq. (30). The self energy is generated to one-loop order from the squared matrix element integrated over available phase space and summed over final states,

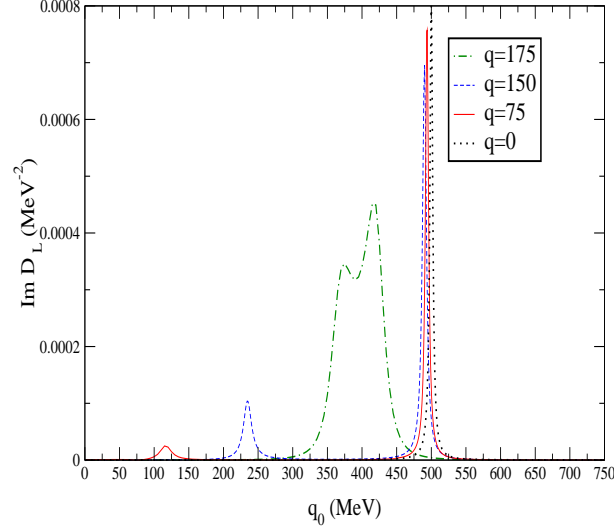


FIG. 8. The imaginary part of the longitudinal ρ propagator for fixed m_S , m_T and various values for the 3-momentum q . The upper ('+') mode is dominant except when q is very close to $q_{\max} = 176.5$ MeV.

$$-\text{Im}\Sigma_{\pi\pi}(q_0, q) = \frac{1}{2} \sum_f \int d\Pi_f (\mathcal{T}\mathcal{T}^*) , \quad (48)$$

with the reduced matrix element $\mathcal{T} = ig_{\rho\pi\pi}\epsilon_\rho^\mu(2q+k)_\mu$, ϵ_ρ^μ the ρ polarization vector and $g_{\rho\pi\pi} = g_{T,S}$ for $\mu = 0, i$, respectively. Focusing on the decay of the V^8 component (ρ^0), which alone couples to the photon, the only nonzero antisymmetric structure constants are f^{128} and f^{458} , representing two independent decay channels which must be added incoherently. The imaginary part of the components of the self energy as computed from eq. (48) are then

$$\begin{aligned} \text{Im}\Sigma_{\pi\pi}^{00}(M) &= \text{Im}\Sigma_{\pi\pi}^L(M)(P_L^{00} + P_T^{00}) \\ \text{Im}\Sigma_{\pi\pi}^{0i}(M) &= \sqrt{\text{Im}\Sigma_{\pi\pi}^L(M)\text{Im}\Sigma_{\pi\pi}^T(M)}(P_L^{0i} + P_T^{0i}) \\ \text{Im}\Sigma_{\pi\pi}^{ij}(M) &= \text{Im}\Sigma_{\pi\pi}^T(M)(P_L^{ij} + P_T^{ij}) \end{aligned} \quad (49)$$

with

$$\begin{aligned} \text{Im}\Sigma_{\pi\pi}^L(M) &= -\frac{g_T^2 M^2}{32\pi} \\ \text{Im}\Sigma_{\pi\pi}^T(M) &= -\frac{g_S^2 M^2}{32\pi} . \end{aligned} \quad (50)$$

We now see that the self-energy is not transverse ($q_\mu\Sigma^{\mu\nu} \neq 0$) unless $g_S = g_T$. This observation enforces the equality of the two couplings (denoted henceforth by g), and therefore the equality of the self-energies (henceforth denoted by $\Sigma_{\pi\pi}$). The self-energies are resummed through a Schwinger-Dyson equation, yielding longitudinal and transverse ρ -propagators of the form

$$D_L(M, q) = \frac{1}{M^2 - m_S^2 \frac{q_0^2}{M^2} + m_T^2 \frac{q^2}{M^2} - \text{Re}\Sigma_{\pi\pi} - i\text{Im}\Sigma_{\pi\pi}} , \quad (51)$$

$$D_T(M, q) = \frac{1}{M^2 - m_S^2 - \text{Re}\Sigma_{\pi\pi} - i\text{Im}\Sigma_{\pi\pi}} . \quad (52)$$

The real parts of the self energy are more involved and could be obtained from subtracted dispersion relations. We will assume that they do not significantly alter the pole structure. Combining eqs. (40), (51) and (52) provides an expression for the thermal emission rate (as a function of the four-momentum q^μ) from the ρ contribution. Numerical

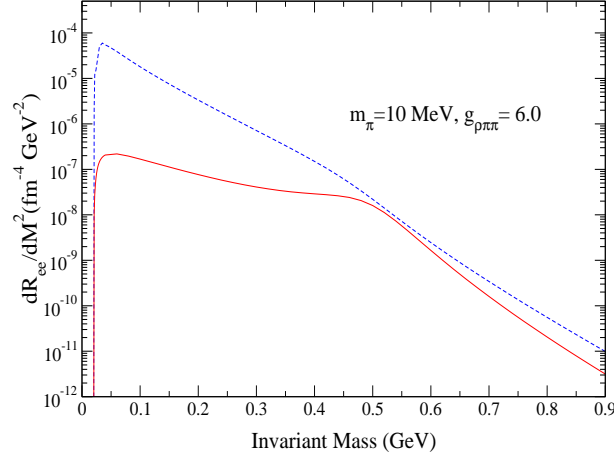


FIG. 9. Invariant-mass spectrum from the longitudinal (dotted) and transverse (solid) modes of propagation of the ρ meson in the CFL phase (pion mass $m_\pi = 10$ MeV) for $\mu_q = 350$ MeV, $T = 80$ MeV and $g_{\rho\pi\pi}$ set to the vacuum value of 6.0. The broad peaks of the longitudinal and transverse mode are discernible around 475 MeV.

integration over 3-momentum yields the rate dR/dM^2 as a function of invariant mass, cf. Fig. 9, where we also included a finite pion mass. The pion mass arises from a non vanishing current quark mass matrix and has been estimated at around $m_\pi \simeq 10$ MeV to leading log accuracy within a Bethe-Salpeter approach for the pionic bound state energy [28]. It simply introduces an extra phase space factor of $(1 - 4m_\pi^2/M^2)^{3/2}$ into the imaginary part of the self-energy, which leads to a notable suppression of the rate only for invariant masses $M \lesssim 50$ MeV. Beyond that, the M^2 dependence of the (imaginary part of the) self energy causes a slight downward shift of the transverse ρ peak below its nominal mass at $M = m_\rho$ (this feature might not persist upon inclusion of corrections to the real part of Σ_T). A close inspection of the denominator in the longitudinal propagator reveals that it also peaks somewhat below $M = m_\rho$ in the invariant-mass spectrum. Numerical values for m_ρ and m_T follow from eqs. (31) and (32) with VMD enforced ($a_T = a_S = 2$), and F_T given to leading logarithm accuracy by [28]

$$F_T^2 \simeq \frac{\mu^2}{\pi^2} \frac{8x_0^2 + \pi^2(1 - \exp(-2x_0))}{4x_0^2 + \pi^2}, \quad x_0 = \frac{3\pi^2}{\sqrt{2}g}. \quad (53)$$

The magnitude of the generalized ρ -meson contribution is compared to the perturbative quark rate in Fig. 10. The former dominates over the latter in the invariant-mass region up to about 0.7 GeV, emphasizing the role of composite (i.e., generalized mesonic) degrees of freedom. Even the one-loop CFL corrections to the quark rate as calculated in sect. II can compete with effective theory results only for sufficiently large pairing gaps, cf. Figs. 3 and 5.

IV. COMPARISON TO LOW-DENSITY APPROACHES

The evaluation of the electromagnetic emissivities in the previous two sections applies to densities large enough to support the formation of superconducting quark matter. More specifically, we assumed the Cooper pairing to follow the symmetry pattern of color-flavor locking. Towards lower chemical potentials the color superconducting matter will undergo a (possibly first order) transition into ordinary hadronic matter⁹, which, nevertheless, is likely

⁹For realistic values of the strange quark mass, $m_s \simeq 100 - 150$ MeV, the CFL phase might well turn into the 2-flavor superconductor (2SC) before hadronic matter is recovered; the one-loop photon self energy for the 2SC state could be calculated along similar lines as done in sect. II, whereas the HLS construction of Sect. III does not apply due to the absence of chiral symmetry breaking. On the other hand, if the 2SC window on the μ_q axis does not exist, the possibility for a continuous transition from CFL to hadronic matter has been raised. Such a scenario would in fact corroborate the evidence for duality that we are about to discuss in terms of the electromagnetic response.

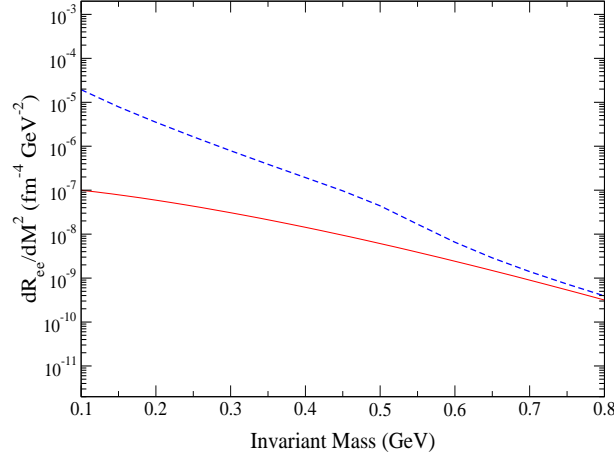


FIG. 10. Dilepton rate (dashed line) including the peak from the generalized ρ meson for $\mu_q = 350$ MeV, $T = 80$ MeV and $\Delta = 10$ MeV. The solid line represents the free $q\bar{q}$ annihilation rate at order α_s^0 at that temperature and density. The ρ peak enhances significantly the rate from the paired quarks.

to occur at densities well above that of normal nuclear matter where hadronic medium effects will be substantial. A natural question to ask then is, how the CFL emissivities compare to results from dense hadronic phases at low temperatures, which should be thought of as an extrapolation from the low density side. Similar comparisons have been discussed before for both photon and dilepton rates at large temperatures ($T = 150 - 200$ MeV) with [24,49] and without [40,25,26] the inclusion of baryon density effects. The low temperature and high density dilepton case (for $T = 80$ MeV and $n_B = 3.5n_0$ corresponding to a quark chemical potential of $\mu_q = 290$ MeV) is exemplified in Fig. 11, where the CFL rates (the combined contribution from the previous two sections) are confronted with in-medium hadronic calculations based on ref. [24,50], as well as the pertinent lowest order results, i.e., perturbative $\mathcal{O}(\alpha_s^0)$ $q\bar{q}$ as well as free $\pi^+\pi^-$ annihilation. The latter two are obviously very different in shape, but upon the inclusion

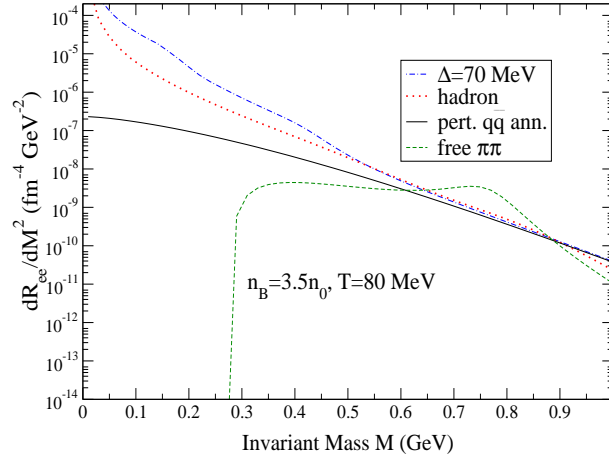


FIG. 11. Comparison of dilepton rates in the in medium hadronic and high density approaches, suggestive of a quark-hadron duality picture holding in dense matter.

of interactions, it appears intriguing that the rates from the two in principle very different ground states exhibit a remarkable tendency to coincide within a factor of two (somewhat more towards very low masses below 300 MeV or so). This agreement opens the possibility that the dilepton signal from the baryon-dense hadronic phase smoothly matches the description within the plasma phase, i.e., the ‘bottom-up’ and ‘top-down’ extrapolations support the

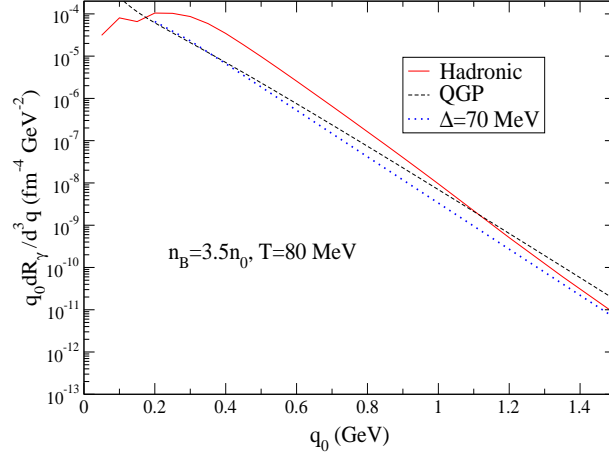


FIG. 12. Photon rates from CFL quark matter, a QGP and a dense hadronic environment at equivalent densities.

emergence of duality.

Another important issue in this context is the one of chiral symmetry restoration. This obviously requires an evaluation of the axial vector current correlation function. Although chiral symmetry in the CFL phase is broken, it has been found in ref. [28] that, to leading logarithm accuracy, the masses of the generalized vector and axial vector mesons are degenerate, $M_V = M_A \simeq 2\Delta(1 - e^{-C/g})^{1/2}$ with $C = (3 - \sqrt{3})\pi^2\sqrt{6}$. This is possible due to the more involved symmetry breaking pattern (as compared to the usual vacuum case), which, e.g., does not require a finite value for the two-quark condensate, but only a nonzero chiral four-quark condensate. The leading $\log \rho$ - a_1 degeneracy is also consistent with our earlier statement that to this accuracy, there is no coupling of the vector current to two-pion states. Although the simplest version of the HLS approach (as constructed in Sect III) does not incorporate explicit axial vector degrees of freedom, it can be accordingly extended [51], which will not be attempted here. We furthermore note that model calculations [2,3] indicate certain chiral breaking effects in the CFL ground state to be substantially weaker than in the vacuum. For e.g., 'constituent' quark masses turn out to be about an order of magnitude smaller than the pairing gaps $\Delta \simeq 100$ MeV. On the other hand, the pion decay constant, which also constitutes an order parameter of spontaneous chiral breaking, is parametrically large, $(F_T^2 = 3 F_S^2 \simeq \mu_q^2/\pi^2)$, i.e., of order $\mathcal{O}(g^0 \mu_q^2)$. Thus the question arises how this can be reconciled with the Weinberg sum rules [52]. One of them relates the pion decay constant to the integrated difference in spectral strengths for vector and axial vector correlators,

$$f_\pi^2 = - \int \frac{dq_0^2}{\pi} \frac{1}{q_0^2} (\text{Im} \Pi_V(q_0) - \text{Im} \Pi_A(q_0)) \quad (54)$$

and has been shown to hold in the medium as well [53]. A near degeneracy of $\text{Im} \Pi_V$ and $\text{Im} \Pi_A$ implies a small pion decay constant. This discrepancy has been resolved in ref. [54], being associated with genuine two-loop diagrams involving an intermediate gluon propagator ('dumbbell diagram'). Naively, these diagrams are of higher order in g , but an infrared singularity in the gluon propagator, being regulated upon resummation by the standard Debye-/Meissner masses, turns them into order $\mathcal{O}(g^0)$ contributions. This lifts the V - A degeneracy and restores the sum rule eq. (54).

Finally, turning to thermal photon production, Fig. 12 compiles rates from the CFL, in-medium hadronic [24] and (perturbative) QGP phase [41]. Here, too, the emission pattern from the dense quark system is quite similar to that computed in hadronic or QGP scenarios.

V. CONCLUSIONS

In this article we have investigated the electromagnetic response of color superconducting quark matter for three massless flavors in the so-called CFL realization. Two approaches were pursued to calculate the e.m. current correlator.

The first one consisted of a perturbative one-loop calculation in terms of the appropriate quark (hole) quasiparticles. In contrast to the free Fermi gas case, where imaginary parts arising from Landau damping are purely spacelike, the

presence of finite quark gaps induces a non-vanishing strength (imaginary part) in the timelike region, thus opening up the possibility for dilepton production. More quantitatively, taking as a baseline the free quark-antiquark annihilation process, quark gaps on the order of 50 MeV lead to appreciable contributions in the 3-momentum integrated dilepton rate up to invariant masses as large as 400 MeV.

The second approach was based on effective field methods built on the notion of spontaneous chiral symmetry breaking in the CFL ground state. After identifying the suitable set of eight generalized Goldstone bosons, a chiral Lagrangian has been constructed with massive vector mesons introduced using the hidden local symmetry technique. Vector meson dominance arises as a natural parameter choice within this framework. The resulting dilepton rates, corresponding to the annihilation of generalized pions via generalized ρ mesons, receive contributions from both the spin-transverse and -longitudinal modes, the latter being dominant for invariant masses below 450 MeV. Both modes have a typical mass around 500 MeV.

Furthermore, we argued that the absence of a pion coupling to the vector current in the leading log approximation implies that both perturbative and effective Lagrangian contribution add to the e.m. correlator. Extrapolating the obtained dilepton rates down to moderate densities, we find them to be comparable (within a factor of 2 or so) with in-medium hadronic calculations as available in the literature. The two generic features shared in both pictures are (i) a strong low mass enhancement originating from soft many-body excitations, and (ii) a rather structureless 'continuum' beyond invariant masses of about 0.5 GeV. This extends the notion of 'quark-hadron duality' into the baryon-dense regime at low temperatures, similar to what has been suggested before for the high temperature case. Our analysis can and should be extended to the 2SC phase, as well as the crystalline phases of dense QCD at low temperature [55,56]. The results should prove useful for a way to probe/discriminate the QCD phase diagram at low temperature and moderate densities, using electromagnetic signals potentially accessible to future heavy-ion experiments, in a way that complements the current hadronic calculations.

ACKNOWLEDGEMENTS

We thank Thomas Schäfer for discussions. This work was supported by the US-DOE grant DE-FG0288ER40388.

-
- [1] K. Rajagopal and F. Wilczek, "The condensed matter physics of QCD", **hep-ph/0011333**; to appear in *"At the Frontier of Particle Physics/handbook of QCD"*, M. Shifman, ed., (World Scientific).
 - [2] M. Alford, K. Rajagopal and F. Wilczek, Nucl. Phys. **B537** (1999) 443.
 - [3] R. Rapp, T. Schäfer, E. V. Shuryak and M. Velkovsky, Ann. of Phys. **280** (2000) 35.
 - [4] K. Rajagopal, Nucl. Phys. **A642** (1998) 26.
 - [5] C. Manuel and K. Rajagopal, eprint **hep-ph/0107211**.
 - [6] HADES, Technical Proposal, GSI 1994;
J. Friese et al., Nucl. Phys. **A654** (1999) 1017.
 - [7] C. Gale and J. Kapusta, Nucl. Phys. **B357** (1991) 65.
 - [8] G. Chanfray and P. Schuck, Nucl. Phys. **A555** (1993) 329.
 - [9] M. Herrman, B. Friman and W. Nörenberg, Nucl. Phys. **A560** (1993) 411.
 - [10] C. Gale and P. Lichard, Phys. Rev. **D49** (1994) 3338
 - [11] G. Chanfray, R. Rapp and J. Wambach, Phys. Rev. Lett. **76** (1996) 368;
R. Rapp, G. Chanfray and J. Wambach, Nucl. Phys. **A617** (1997) 472.
 - [12] J.V. Steele, H. Yamagishi and I. Zahed, Phys. Lett. **B384** (1996) 255.
 - [13] J.V. Steele, H. Yamagishi and I. Zahed, Phys. Rev. **D56** (1997) 5605;
J.V. Steele and I. Zahed, Phys. Rev. **D60** (1999) 037502.
 - [14] F. Klingl, N. Kaiser and W. Weise, Nucl. Phys. **A624** (1997) 527.
 - [15] R. Rapp and J. Wambach, Adv. Nucl. Phys. **25** (2000) 1.
 - [16] L. McLerran and T. Toimela, Phys. Rev. **D31** (1985) 545.
 - [17] J. Cleymans, J. Fingberg and K. Redlich, Phys. Rev. **D35** (1987) 2153.
 - [18] P. Altherr and P. Aurenche, Z. Phys. **C45** (1989) 99.
 - [19] E. Braaten, R. Pisarski and T.C. Yuan, Phys. Rev. Lett. **64** (1990) 2242.
 - [20] A. Peshier and M. Thoma, Phys. Rev. Lett. **84** (2000) 841.

- [21] I. Zahed, *Light Relativistic Bound States at High Temperature, Thermal Field Theories*, Eds. H. Ezawa et al., North Holland (Amsterdam, 1991), p. 357.
- [22] C.H. Lee, T. Wirstam, I. Zahed and H. Hansson, Phys. Lett. **B448** (1999) 168.
- [23] A. Schäfer and M. Thoma, Phys. Lett. **B451** (1999) 195.
- [24] R. Rapp, Nucl. Phys. **A661** (1999) 33;
R. Rapp and J. Wambach, Eur. Phys. J. **A6** (1999) 415.
- [25] A.V. Leonidov and P.V. Ruuskanen, Eur. Phys. J. **4** (1998) 519.
- [26] C.H. Lee, H. Yamagishi and I. Zahed, Phys. Rev. **C58** (1998) 2899.
- [27] D.K. Hong, M. Rho and I. Zahed, Phys. Lett. **B468** (1999) 261
- [28] M. Rho, E. Shuryak, A. Wirzba and I. Zahed, Nucl. Phys **A676** (2000) 273
- [29] R. Casalbuoni and R. Gatto, Phys. Lett. **B464** (1999) 111
- [30] D.T. Son and M.A. Stephanov, Phys. Rev. **D 61** (2000) 074012
- [31] D.F. Litim and C. Manuel, Phys. Rev. **D64** (2001) 094013
- [32] D.H. Rischke, Phys. Rev. **D62** (2000) 034007
- [33] R.D. Pisarski and D.H. Rischke, Phys. Rev. **D60** (1999) 094013
- [34] I.A. Shovkovy and L.C.R. Wijewardhana, Phys. Lett. **B470** (1999) 189
- [35] K. Zarembo, Phys. Rev. **D62** (2000) 054003
- [36] T. Schäfer and F. Wilczek, Phys Rev. **D60**, (1999) 114033
- [37] M. Alford, J. Berges and K. Rajagopal, Nucl. Phys. **B571** (2000) 269
- [38] G.W. Carter and S. Reddy, Phys. Rev. **D62** (2000) 103002
- [39] T. Schäfer and F. Wilczek, Phys. Rev. Lett. **82** (1999) 3956
- [40] J.I. Kapusta, P. Lichard and D. Seibert, Phys. Rev. **D44** (1991) 2774.
- [41] P. Arnold, G.D. Moore and L.G. Yaffe, eprint hep-ph/0111107.
- [42] M. Bando, T. Kugo and K. Yamawaki, Nucl. Phys. **B 259** (1985) 493
- [43] M. Bando, T. Kugo and K. Yamawaki, Prog. Theor. Phys. **73** (1985) 1541
- [44] M. Bando, T. Kugo, S. Uehara, K. Yamawaki and T. Yanagida, Phys. Rev. Lett **54** (1985) 1215
- [45] T. Fujiwara, T. Kugo, H. Terao, S. Uehara and K. Yamawaki, Prog. Theor. Phys. **73** (1985) 926.
- [46] D. K. Hong, Nucl. Phys. **B582** (2000) 451
- [47] M. Harada and K. Yamawaki, Phys. Rev. Lett. **87** (2001) 152001
- [48] M. Le Bellac, *Thermal Field Theory*, (Cambridge University Press) 1996
- [49] R. Rapp, Phys. Rev. **C63** (2001) 054907.
- [50] M. Urban, M. Buballa R. Rapp and J. Wambach, Nucl. Phys. **A673** (2000) 357
- [51] M. Bando, T. Fujiwara and K. Yamawaki, Prog. Theor. Phys. **79** (1988) 1140.
- [52] S. Weinberg, Phys. Rev. Lett. **18** (1967) 507.
- [53] J. Kapusta and E.V. Shuryak, Phys. Rev. **D49** (1994) 4694.
- [54] C. Manuel and M.H.G. Tytgat, Phys. Lett. **501** (2001) 200.
- [55] R. Rapp, E. Shuryak and I. Zahed, Phys. Rev. **D63** (2001) 034008.
- [56] J.A. Bowers, J. Kundu, K. Rajagopal and E. Shuster, Phys. Rev. **D64** (2001) 014024.